scientific reports

Check for updates

OPEN

Thermal stable properties of solid hybrid nanoparticles for mixed convection flow with slip features

Liaquat Ali Lund[1], Maha M. A. Lashin[2], Ubaidullah Yashkun[3], Kamel Guedri[4], Sami Ullah Khan[5], M. Ijaz Khan[6,7]✉, Omar T. Bafakeeh[8] & Poom Kumam[9,10]✉

Following to improved thermal impact of hybrid nanomaterials, wide range applications of such materials is observed in the thermal engineering, extrusion systems, solar energy, power generation, heat transfer devices etc. The hybrid nanofluid is a modified form of nanofluid which is beneficial for improving energy transfer efficiency. In current analysis, the solid nanoparticles aluminium ($\phi_{Al_2O_3}$) and copper (ϕ_{Cu}) have been mixed with water to produce a new hybrid nanofluid. The investigation of a steady two-dimensional mixed convection boundary layer flow of the resultant hybrid nanofluid on a vertical exponential shrunk surface in the existence of porous, magnetic, thermal radiation, velocity, and thermal slip conditions is carried out. Exponential similarity variables are adopted to transform the nonlinear partial differential equation into a system of ordinary differential equations which has been then solved by employing the shooting method in Maple software. The obtained numerical results such as coefficient of skin friction $f''(0)$, heat transfer rate $-\theta'(0)$, velocity $f'(\eta)$ and temperature $(\theta(\eta))$ distributions are presented in the form of different graphs. The results revealed that duality exists in solution when the suction parameter $S \geq S_{ci}$ in assisting flow case. Due to non-uniqueness of solutions, a temporal stability analysis needs to be performed and the result indicates that the upper branch is stable and realizable compared to the lower branch.

List of symbols

K^*	Permeability of porous medium
T	Temperature of fluid
T_∞	Free stream temperature
ρ_{hnf}	Density
k_{hnf}	Thermal conductivity
u_w	Surface velocity
D	Thermal slip factor
λ_1	I mixed parameter
K	Parameter of porosity
Nu_x	Local Nusselt number
δ_T	Thermal slip parameter
Rd	Thermal radiation parameter
B_0	Magnetic field c strength

[1]School of Quantitative Sciences, Universiti Utara Malaysia, 06010 Sintok, Kedah, Malaysia. [2]College of Engineering, Princess Nourah bint Abdulrahman University, Riyadh, Saudi Arabia. [3]Department of Mathematics and Social Sciences, Sukkur IBA University, Sukkur, Pakistan. [4]Mechanical Engineering Department, College of Engineering and Islamic Architecture, Umm Al-Qura University, P.O. Box 5555, Mecca 21955, Saudi Arabia. [5]Department of Mathematics, COMSATS University Islamabad, Sahiwal 57000, Pakistan. [6]Department of Mathematics and Statistics, Riphah International University I-14, Islamabad 44000, Pakistan. [7]Mathematical Modelling and Applied Computation Research Group (MMAC), Department of Mathematics, King Abdulaziz University, Jeddah, Saudi Arabia. [8]Department of Industrial Engineering, Jazan University, Jazan 82822, Saudi Arabia. [9]Center of Excellence in Theoretical and Computational Science (TaCS-CoE) and KMUTT Fixed Point Research Laboratory, Room SCL 802 Fixed Point Laboratory, Science Laboratory Building, Departments of Mathematics, Faculty of Science, King Mongkut's University of Technology Thonburi (KMUTT), 126 Pracha-Uthit Road, Bang Mod, Thung Khru, Bangkok 10140, Thailand. [10]Department of Medical Research, China Medical University Hospital, China Medical University, Taichung 40402, Taiwan. ✉email: mikhan@math.qau.edu.pk; poom.kum@kmutt.ac.th

$T_w(x)$	Temperature of surface
$(\rho c_p)_{hnf}$	Effective heat capacity
σ_{hnf}	Electrical conductivity
μ_{hnf}	Viscosity
A	Velocity slip factor
S	Parameter of blowing/suction
M	Hartmann number
δ	Velocity slip parameter
Pr	Prandtl number
C_f	Skin friction coefficient

From last few years, the investigation of fluid dynamics has attracted considerable much attention amongst analysts and scholars from various fields because of its enormous potential applications in engineering, designing, science, innovation, and technology. The most frequently discussed topics are related to boundary layer flow which was initially discovered by Ludwig Prandtl. Since then, many scholars had attempted to study numerous types of Newtonian and non-Newtonian fluids with different characteristics and sheets. Hakeem et al.[1] investigated the effect on heat transfer of a Casson fluid by using of inclined magnetized field. They concluded that the aligned angle role in regulating the magnetic strength in the Casson fluid flow area is essential. When the aligned magnetic field values increase, both Nusselt number and the coefficient of skin friction decrease, while the temperature of the non-dimensional surface raises. Mandal et al.[2] examined the thermal radiation effect on the micropolar fluid. They deduced that as the value of mixed convection parameter inclines, the flow velocity tends to increase, but both temperature and angular velocity seem to decline. Meanwhile, Shahzad et al.[3] premeditated the effect of heat transfer of axisymmetric flow of magnetized fluid on an exponentially stretching surface. It is noticed that the velocity of radial increases when the suction and magnetic parameters are increased.

In convection, the heat transfer occurs through mass movement of fluid molecules (gases or liquids). It takes place above the hot surface where the heated fluid molecules become less dense and move from one place to another, taking heat within them due to the difference in temperature. convection is a major source of heat transfer that happens through diffusion or advection or both[4]. For an example, the convection exists in the cooling of the electronic parts of the computer. A small fan is installed to the side or rear of chassis to cool the electronic components with openings on the side surface for easy air circulation. There are three kinds of convection. In free convection, the flow of heat transfer takes place due to body forces that happen because of density changes that arise due to the temperature difference in the flow filed. This is an important mode of heat transfer and widely used in engineering and industrial applications. Forced convection, on the hand, occurs when the temperature of the solid surface and the fluid are different. The heat is transmitted as a forced convection from the hotter to the colder regime. According to Waini et al.[5], "the fluid motion for the case of forced convection is due to an external motive source such as a fan or pump. The phenomena of forced convection are also very important and have many applications in industry such as the radiator system in vehicles, heating, and cooling of parts of the body by blood circulation". Meanwhile, mixed convection is a mixture of forced and free convection. It is a very efficient mechanism of heat transmission that occurs in a wide variety of transport processes in both engineered devices and nature. In mixed convection both free and forced convection act together in the process of heat transfer[6]. It is most likely that Merkin[7] is the first researcher who considered a mixed convection effect on boundary layer flow for multiple solutions. Later in 1986, he extended his work to porous medium and found dual solutions[8]. Ahmad et al.[9] further explored the concept of mixed convection flow on nanofluid and stated that there is no uniqueness of solutions within a limited range of parameters.

Recently, invention of the advanced heat transfer fluids acquired attention in the field of science and technology. One of these fluids is hybrid nanofluid which is also referred as a modern type of nanofluid. Since nanofluid is a blend of solid nanoparticles in the base fluid as stated in Choi and Eastman[10] while hybrid nanofluid is the blend of nanoparticles in a base nanofluid in which nanofluid particles should be distinct. Avramenko and Shevchuk[11] discussed the self-similar approach to the heat and mass transfer phenomenon associated to the nanofluid problem. Avramenko and Shevchuk[12] reported the thermal impact of nanomaterials in absence of condensation and boiling phenomenon. Gowda et al.[13] observed the vertically moving disk supported with decomposition of hybrid nanoparticles. Kumar et al.[14] studied the cylindrical flow of ferromagnetic nanoparticles with significant contribution of magnetic dipole. Radhika et al.[15] discussed the hybrid nanoparticles suspension with dust particles confined by melting surface. Kumar et al.[16] discussed the rotating surface flow in upward and downward moving disk subject to the hybrid nanofluids. Gowda et al.[17] contributed the Dufour features towards the nanofluid numerically. The Marangoni convection flow of nanofluid with binary chemical reaction was evaluated by Gowda et al.[18]. Haq et al.[19] depicted a theoretical thermal visualization of hybrid nanofluid problem with permeable cylinder. The fractional based mathematical model for hybrid nanofluid has been worked out by Wang et al.[20]. Lund et al.[21] performed a stability measurement of nanofluid via shrinking surface. Yan et al.[22] proposed the heating impact of nanofluid with imposition of multiple slip effects.

The aim of current continuation is to express the thermal dynamic of hybrid nanofluid due to vertically space when multiple slip effects are significant. The novelty of current work is justified as:

- The thermal impact of hybrid nanofluid with utilization of copper and aluminium oxide nanoparticles with water base fluid.
- The mixed convection, thermal raidation and magnetic force influences are contributed.

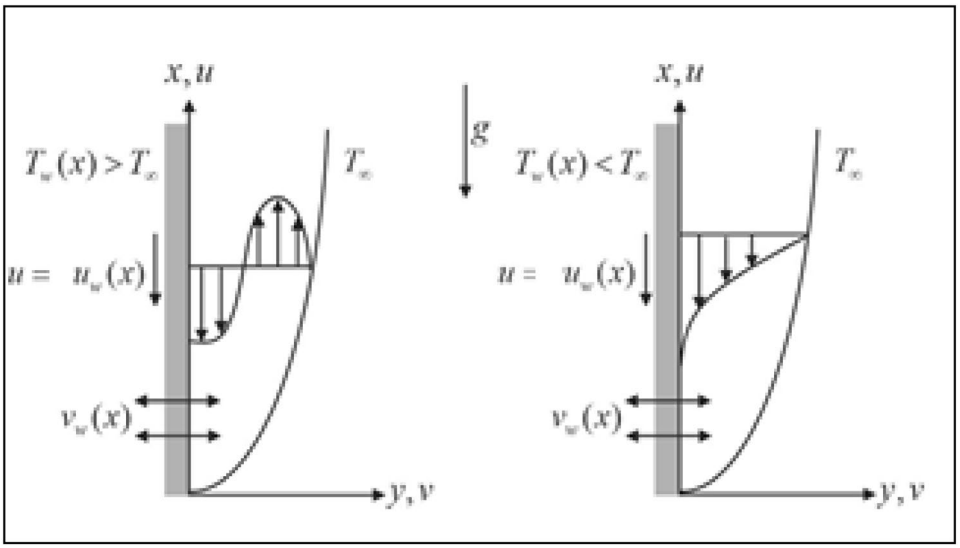

Figure 1. Physical model of the problem.

- The hybrid nanofluid is impacted with multiple velocity and thermal flow constraints. The motivations for consideration such slip features are associated to control of hybrid nanofluid velocity and thermal performances.
- The stability of hybrid nanoparticles is evaluated and evaluated. It is emphasized that various thermal models on nanofluid are available in the literature, however, the stability framework of such models is not ensured in most of investigations.
- The velocity and thermal profiles are observed in distinct flow regimes.
- The numerical prediction of flow model are captured with shooting technique.

Mathematical description of problem

Let us consider 2D, steady mixed convection and incompressible flow of hybrid nanofluid with effect of porous medium, thermal radiation over a vertical exponentially shrinking sheet (refer to Fig. 1). The governing equations are simplified via boundary layer theory[23]. Moreover, the uniform magnetic field of strength B is applied normal to a shrinking sheet. The governance model with all assumptions are as follows[20–22]:

$$\frac{\partial u}{\partial x} + \frac{\partial v}{\partial y} = 0 \tag{1}$$

$$u\frac{\partial u}{\partial x} + v\frac{\partial u}{\partial y} = \frac{\mu_{hnf}}{\rho_{hnf}}\frac{\partial^2 u}{\partial y^2} + \beta_{hnf} g(T - T_\infty) - \frac{1}{\rho_{hnf}}\left(\frac{\mu_{hnf}}{K^*} + \sigma_{hnf} B^2\right)u \tag{2}$$

$$u\frac{\partial T}{\partial x} + v\frac{\partial T}{\partial y} = \left[\frac{k_{hnf}}{(\rho c_p)_{hnf}} + \frac{16\sigma_1 T_\infty^3}{3k^*(\rho c_p)_{hnf}}\right]\frac{\partial^2 T}{\partial y^2} \tag{3}$$

with boundary conditions[20,21]:

$$\begin{cases} v = v_w(x), u = u_w + A\vartheta_f \frac{\partial u}{\partial y}, T = T_w + D\frac{\partial T}{\partial y} & \text{as } y = 0 \\ u \to 0, T \to T_\infty, & \text{as } y \to \infty \end{cases}. \tag{4}$$

The velocities of y and x axis are denoted by v and u accordingly, $K^* = K_0^* e^{-x/l}$ shows the permeability of porous medium, $B = B_0 e^{x/2l}$ is the magnetic field along with constant magnetic strength $e^{x/2l}$, T is the temperature of fluid, $T_w(x) = T_\infty + T_0 e^{2x/l}$ is the temperature of surface where T_∞ is free stream temperature, $(\rho c_p)_{hnf}$, ρ_{hnf}, σ_{hnf}, k_{hnf}, and μ_{hnf}, are the effective heat capacity, density, electrical conductivity, thermal conductivity and viscosity of the considered hybrid nanofluid. In addition, $u_w = -U_w e^{x/l}$ is the surface velocity,$A = A_1 e^{-x/2l}$ is velocity slip factor, $D = D_1 e^{-x/2l}$ is thermal slip factor, and $v_w = \sqrt{\frac{\vartheta_f U_w}{2l}} e^{x/2l} S$ where S is the parameter of blowing/suction.

In this study the thermophysical properties of nanomaterials, base fluid, and hybrid nanofluid are used. In relation to, Tables 1 and 2 are presented[20,21].

The following similarity transformation variables will be adopted to convert the system of equations into ODEs[20,21].

Properties	Hybrid nanofluid
Dynamic viscosity	$\mu_{hnf} = \frac{\mu_f}{\left(1-\phi_{Al_2O_3}\right)^{2.5}(1-\phi_{Cu})^{2.5}}$
Density	$\rho_{hnf} = (1-\phi_{Cu})\left[\left(1-\phi_{Al_2O_3}\right)\rho_f + \phi_{Al_2O_3}\rho_{Al_2O_3}\right] + \phi_{Cu}\rho_{Cu}$
Thermal conductivity	$k_{hnf} = \frac{k_{Cu}+2k_{nf}-2\phi_{Cu}\left(k_{nf}-k_{Cu}\right)}{k_{Cu}+2k_{nf}+\phi_{Cu}\left(k_{nf}-k_{Cu}\right)} \times \left(k_{nf}\right)$ where $k_{nf} = \frac{k_{Al_2O_3}+2k_f-2\phi_{Al_2O_3}\left(k_f-k_{Al_2O_3}\right)}{k_{Al_2O_3}+2k_f+\phi_{Al_2O_3}\left(k_f-k_{Al_2O_3}\right)} \times \left(k_f\right)$
Heat capacity	$\left(\rho c_p\right)_{hnf} = (1-\phi_{Cu})\left[\left(1-\phi_{Al_2O_3}\right)\left(\rho c_p\right)_f + \phi_{Al_2O_3}\left(\rho c_p\right)_{Al_2O_3}\right] + \phi_{Cu}\left(\rho c_p\right)_{Cu}$
Electrical conductivity	$\sigma_{hnf} = \frac{\sigma_2+2\sigma_{nf}-2\phi_2\left(\sigma_{nf}-\sigma_2\right)}{\sigma_2+2\sigma_{nf}+\phi_2\left(\sigma_{nf}-\sigma_2\right)} \times \left(\sigma_{nf}\right)@$ where $\sigma_{nf} = \frac{\sigma_1+2\sigma_f-2\phi_1\left(\sigma_f-\sigma_1\right)}{\sigma_1+2\sigma_f+\phi_1\left(\sigma_f-\sigma_1\right)} \times \left(\sigma_f\right)$
Thermal expansion coefficient	$(\beta)_{hnf} = (1-\phi_{Cu})\left[\left(1-\phi_{Al_2O_3}\right)(\beta)_f + \phi_{Al_2O_3}(\beta)_{Al_2O_3}\right] + \phi_{Cu}(\beta)_{Cu}$

Table 1. Thermophysical features of hybrid nanofluid[20,21].

Fluids	Copper (Cu)	Alumina (Al_2O_3)	Water (H_2O)	$\beta \times 10^{-5}$(1/K)
ρ(kg/m^3)	8933	3970	997.1	0.85
c_p(J/kg K)	385	765	4179	1.67
k (W/m K)	400	40	0.613	21

Table 2. The properties of thermos physical[20,21].

$$\psi = \sqrt{2\vartheta_f l U_w}e^{x/2l}f(\eta);\ \theta(\eta) = \frac{T-T_\infty}{T_w-T_\infty};\ \eta = y\sqrt{\frac{U_w}{2\vartheta_f l}}e^{x/2l} \tag{5}$$

where ψ represents the stream function while the velocities are as $u = \frac{\partial\psi}{\partial y}$ and $v = -\frac{\partial\psi}{\partial x}$. Put Eq. (5) in the Eqs. (2–3) yields

$$f''' - Kf' + \xi_1\xi_2\left\{f''f - 2\left(f'\right)^2 + 2\lambda_1\left(\beta_{hnf}/\beta_f\right)\theta\right\} - \frac{\sigma_{hnf}}{\sigma_f}\xi_2 Mf' = 0 \tag{6}$$

$$\frac{1}{Pr\xi_3}\left[\left(k_{hnf}/k_f\right) + \frac{4Rd}{3}\right]\theta'' + \theta' f - 4\theta f' = 0 \tag{7}$$

$$\begin{cases} \xi_1 = \left\{(1-\phi_{Cu})\left[1-\phi_{Al_2O_3} + \phi_{Al_2O_3}\left(\rho_{Al_2O_3}/\rho_f\right)\right] + \phi_{Cu}\left(\rho_{Cu}/\rho_f\right)\right\} \\ \xi_2 = (1-\phi_{Cu})^{2.5}\left(1-\phi_{Al_2O_3}\right)^{2.5} \\ \xi_3 = \left\{(1-\phi_{Cu})\left[1-\phi_{Al_2O_3} + \phi_{Al_2O_3}\frac{(\rho c_p)_{Al_2O_3}}{(\rho c_p)_f}\right] + \phi_{Cu}\frac{(\rho c_p)_{Cu}}{(\rho c_p)_f}\right\} \end{cases} \tag{8}$$

along with boundary conditions

$$\begin{cases} f(0) = S, f'(0) = -1 + \delta f''(0), \theta(0) = 1 + \delta_T\theta'(0) \\ f'(\eta) \to 0; \theta(\eta) \to 0\ as\ \eta \to \infty \end{cases} \tag{9}$$

where $\lambda_1 = \frac{g\beta_f T_0 l}{U_w^2}$ is the mixed parameter, $M = \frac{2l\sigma_f(B_0)^2}{U_w\rho_f}$ is a Hartmann number, $K = \frac{l\mu_f}{U_w\rho_f K_0^*}$ is the parameter of porosity, $\delta = A_1\sqrt{\frac{\vartheta_f U_w}{2l}}$ is the velocity slip parameter,$\delta_T = D_1\sqrt{\frac{U_w}{2\vartheta_f l}}$ is the thermal slip parameter, $Pr = \frac{\vartheta_f}{\alpha_f}$ is Prandtl number, and $Rd = \frac{4\sigma_1 T_\infty^3}{k^* k_f}$ is thermal radiation parameter.

The substantial physical factors skin friction coefficient C_f and local Nusselt number Nu_x are

$$C_f = \frac{\mu_{hnf}}{\rho_f u_w^2}\left(\frac{\partial u}{\partial y}\right)|y=0, \quad Nu_x = -\frac{xk_{hnf}}{k_f(T_w-T_\infty)}\left(\frac{\partial T}{\partial y}\right)|y=0 \tag{10}$$

By using Eq. (5) in Eq. (10) leads to

$$\sqrt{Re}C_f = \frac{1}{\xi_2}f''(0);\ \sqrt{\frac{1}{Re}}Nu_x = -\left[\frac{k_{hnf}}{k_f} + \frac{4Rd}{3}\right] + \theta'(0). \tag{11}$$

Stability analysis

To determine the stable solution a stability analysis is executed. Temporal stability of the solutions is possible when the unsteady model of the Eqs. (2–3) are considered by introducing $\tau = \frac{U_w}{2l}e^{x/l}\cdot t$ as proposed by Weidman et al.[20]. As a result, we have

$$\frac{\partial u}{\partial t} + u\frac{\partial u}{\partial x} + v\frac{\partial u}{\partial y} = \frac{\mu_{hnf}}{\rho_{hnf}}\frac{\partial^2 u}{\partial y^2} + \beta_{hnf}g(T - T_\infty) - \frac{1}{\rho_{hnf}}\left(\frac{\mu_{hnf}}{K^*} + \sigma_{hnf}B^2\right)u \tag{12}$$

$$\frac{\partial T}{\partial t} + u\frac{\partial T}{\partial x} + v\frac{\partial T}{\partial y} = \left[\frac{k_{hnf}}{(\rho c_p)_{hnf}} + \frac{16\sigma_1 T_\infty^3}{3k^*(\rho c_p)_{hnf}}\right]\frac{\partial^2 T}{\partial y^2}. \tag{13}$$

Now, applying the following similarity transformation variables

$$\begin{aligned}\psi &= \sqrt{2\vartheta l U_w}e^{x/2l}f(\eta,\tau);\ \eta = y\sqrt{\frac{U_w}{2\vartheta l}}e^{x/2l};\ \tau = \frac{U_w}{2l}e^{x/l}.t;\ \theta(\eta,\tau)\\ &= (T - T_\infty)/(T_w - T_\infty).\end{aligned} \tag{14}$$

Using (14) on Eqs. (12–13) produces

$$\begin{aligned}&\frac{\partial^3 f(\eta,\tau)}{\partial\eta^3} + \xi_1\xi_2\left\{\frac{\partial^2 f(\eta,\tau)}{\partial\eta^2}f(\eta,\tau) - 2\left(\frac{\partial f(\eta,\tau)}{\partial\eta}\right)^2 - \frac{\partial^2 f(\eta,\tau)}{\partial\tau\partial\eta} + 2\lambda_1\left(\beta_{hnf}/\beta_f\right)\theta(\eta,\tau)\right\}\\ &- \frac{\sigma_{hnf}}{\sigma_f}\xi_2\frac{\partial f(\eta,\tau)}{\partial\eta} - K\frac{\partial f(\eta,\tau)}{\partial\eta} = 0\end{aligned} \tag{15}$$

$$\frac{1}{Pr\xi_3}\left[\left(k_{hnf}/k_f\right) + \frac{4Rd}{3}\right]\frac{\partial^2\theta(\eta,\tau)}{\partial\eta^2} + f(\eta,\tau)\frac{\partial\theta(\eta,\tau)}{\partial\eta} - 4\frac{\partial f(\eta,\tau)}{\partial\eta}\theta(\eta,\tau) - \frac{\partial\theta(\eta,\tau)}{\partial\tau} = 0 \tag{16}$$

with corresponding boundary conditions

$$\begin{cases} f(0,\tau) = S,\ \frac{\partial f}{\partial\eta}(0,\tau) = -1 + \delta\frac{\partial^2 f(0,\tau)}{\partial\eta^2}, \theta(0,\tau) = 1 + \delta_T\frac{\partial\theta(0,\tau)}{\partial\eta} \\ f'(\eta,\tau)\to 0, \theta(\eta,\tau)\to 0 \text{ as } \eta\to\infty \end{cases}. \tag{17}$$

To test stability analysis of solutions, some small perturbation functions are assumed $f(\eta) = f_0(\eta)$ and $\theta(\eta) = \theta_0(\eta)$ such as

$$\theta(\eta,\tau) = \theta_0(\eta) + e^{-\varepsilon\tau}G(\eta,\tau);\ f(\eta,\tau) = f_0(\eta) + e^{-\varepsilon\tau}F(\eta,\tau) \tag{18}$$

here $G(\eta,\tau)$ and $F(\eta,\tau)$ and are the small concerned to $\theta_0(\eta)$. and $f_0(\eta)$ and ε'' is the unknown eigenvalue. Putting Eq. (18) into Eqs. (15–17) where solutions $f(\eta) = f_0(\eta)$ and $\theta(\eta) = \theta_0(\eta)$ of steady state Eqs. (8–9) are found by setting $\tau = 0$. Thus, we get

$$F_0''' + \xi_1\left\{f_0F_0'' + F_0f_0'' - 4f_0'F_0' + 2\lambda_1\left(\beta_{hnf}/\beta_f\right)G_0 + \varepsilon F_0'\right\} - \frac{\sigma_{hnf}}{\sigma_f}\xi_2F_0' - KF_0' = 0 \tag{19}$$

$$\frac{1}{Pr\xi_3}\left[\left(k_{hnf}/k_f\right) + \frac{4Rd}{3}\right]G_0'' + f_0G_0' + F_0\theta_0' - 4f_0'G_0 - 4F_0'\theta_0 + \frac{2Ec}{\xi_2\xi_3}f_0''F_0'' + \varepsilon G_0 = 0 \tag{20}$$

whose boundary conditions are

$$\begin{cases} F_0(0) = 0, F_0'(0) = \delta F_0''(0), G_0(0) = \delta_T G_0'(0) \\ F_0'(\eta)\to 0, G_0(\eta)\to 0 \text{ as } \eta\to\infty \end{cases}. \tag{21}$$

The boundary condition should be reduced to the initial condition to find the ε_1. Hence, we reduced $F_0'(\eta)\to 0$ as $\eta\to\infty$ into $F_0''(0) = 1$.

Validation of results

Before starting to discuss the results of the current study, we have compared coding of a numerical method to ensure that our computer code works properly. The results are verified in Table 3 for limiting flow constraints with work of Lund et al.[21]. A good agreement has been noticed of current results with investigation of Lund et al.[21]. The results are further verified in Table 4 with outcomes of Yan et al.[22]. An outstanding measurement between both results are reported.

	Lund et al.[21]		Present	Results
Pr	$f''(0)$	$\theta'(0)$	$f''(0)$	$\theta'(0)$
1	4.449203	−4.447507	4.449203	−4.447507
1.6	4.540536	−7.334577	4.540536	−7.334577
2	4.570372	−9.284828	4.570372	−9.284828
2.4	4.590011	−11.247347	4.590011	−11.247347
6.2			4.648148	−30.10742

Table 3. Values of $f''(0)$ and $\theta'(0)$ for the various values of Pr by keeping $S = 5, \phi_{Al_2O_3} = \phi_{Cu} = 0$, $\lambda_1 = -0.5, Rd = K = M = \delta = \delta_T = 0$.

	Yan et al.[22]		Present	Results
	Upper branch	Lower branch	Upper branch	Lower branch
ϕ_{Cu}	$f''(0)$		$f''(0)$	
0.01	2.48626	−1.10767	2.48626	−1.10767
0.05	2.81888	−1.62610	2.81888	−1.62610
0.1	3.07486	−2.08072	3.07486	−2.08072

Table 4. Values of $f''(0)$ for the various values of ϕ_{Cu} by keeping $\phi_{Al_2O_3} = 0.1, \lambda_1 = \delta = K = M = 0$ and $S = 3$.

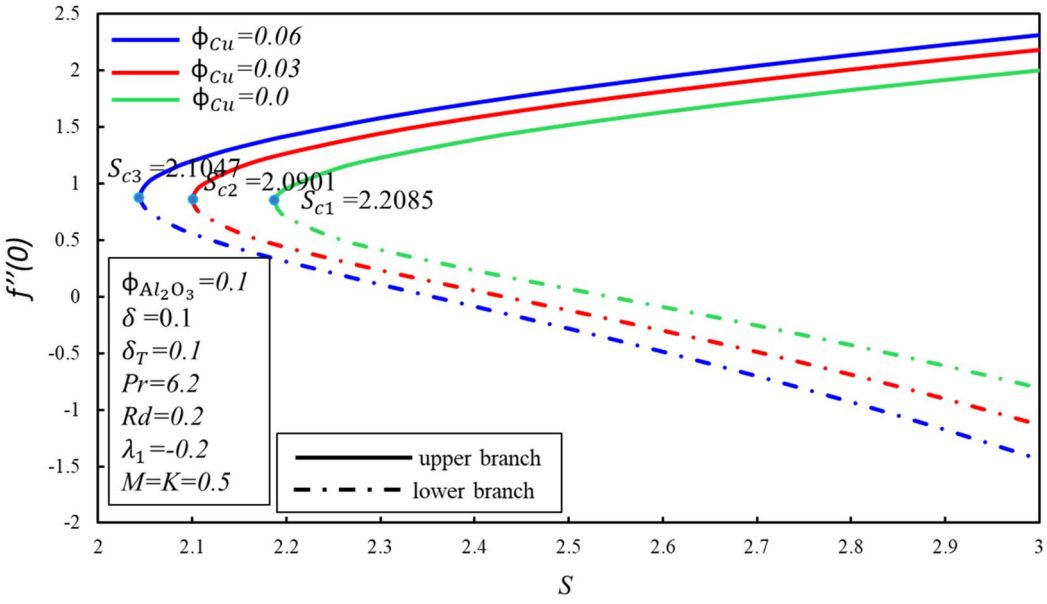

Figure 2. Behavior of $f''(0)$ in impact of ϕ_{Cu}.

Results and discussion

The system of nonlinear ODEs (6–7) subject to boundary condition (9) has been successfully solved using shooting method with 4th order of Runge Kutta process in Maple software. This method has been widely used by numerous academics and scholars to solve fluid flow problems. All over the figures, the solutions duality has been gotten by using various initial guessing for $f''(0)$ and $\theta'(0)$ in which all the profiles of velocity and temperature satisfied the boundary condition $\eta \to \infty$ asymptotically. Throughout this study, we kept a Prandtl number $Pr = 6.2$ for water at 25 °C and the $\phi_{Al_2O_3} = 0.1$ as proposed by Devi and Devi[24]. The range of ϕ_{Cu} is 0 to 0.06. Figures 2 and 3 show the effect of ϕ_{Cu} on behavior of skin friction coefficient $f''(0)$ and rate of heat transfer $-\theta'(0)$, respectively. Both figures portray the dropping characters as ϕ_{Cu} rises in the lower branch. In upper branch, $f''(0)$ increases with ϕ_{Cu} and S. On the other hand, $-\theta'(0)$ rises in both branches when S enhances. It is observed that the fluid is flowing towards S till it arrives a point S_{ci} where $i = 1, 2, 3$, S_{ci} is the critical point of S where the connection of the upper and lower branch exists. No branch exists when $S < S_{ci}$. It is worth

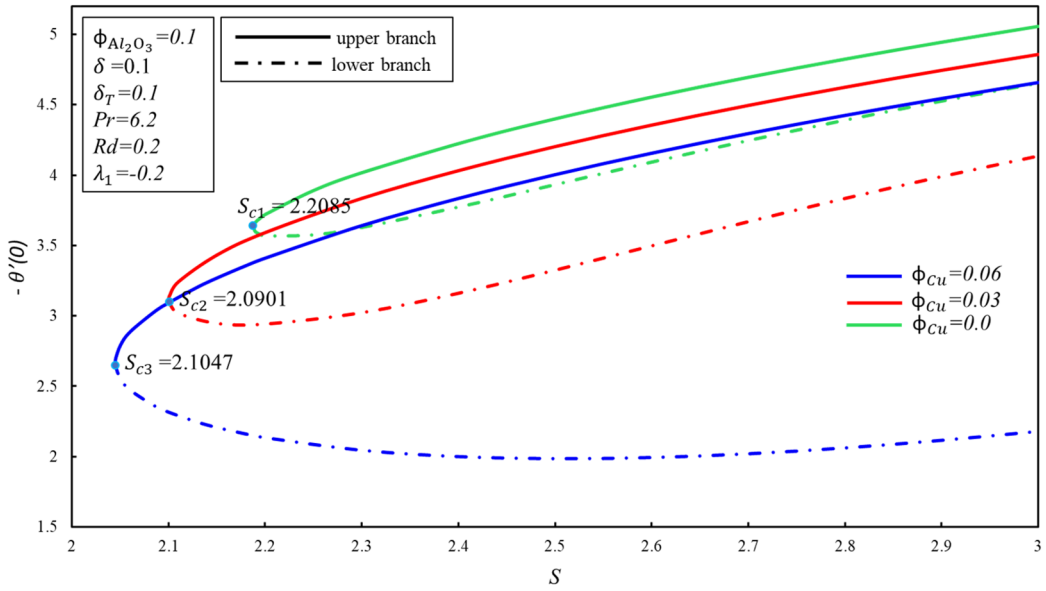

Figure 3. Behavior of $-\theta'(0)$ in impact of ϕ_{Cu}.

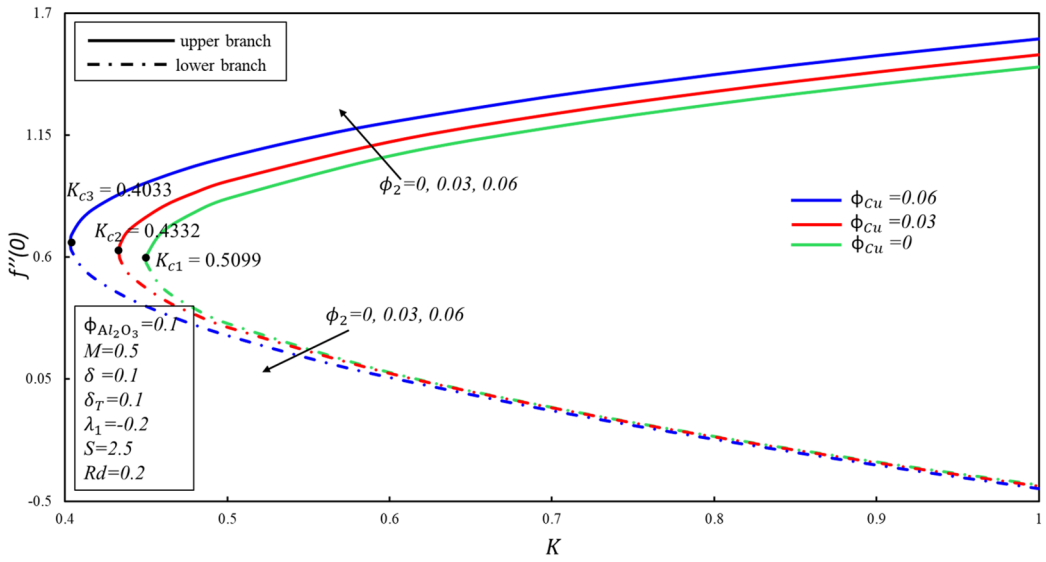

Figure 4. Behavior of $f''(0)$ in impact of ϕ_{Cu}.

mentioning that when $\phi_{\mathrm{Cu}} = 0$, it is purely Al_2O_3 water based nanofluid and $S_{c1} = 2.2085$, after that 3% of ϕ_{Cu} is added and got $S_{c2} = 2.0901$. Additionally, the value of S_{c3} seems to increase as an addition of 6% of the solid volume fraction of ϕ_{Cu} in the hybrid nanofluid. Furthermore, increasing in ϕ_{Cu} extended the separation of layer and the branch range seems to release.

Figures 4 and 5 depicted the porosity parameter K on the magnitude of $f''(0)$ and $-\theta'(0)$ for different values of ϕ_{Cu}. The corresponding critical values of ϕ_{Cu} are K_c and K_c denotes critical point at which both branches exist. Dual branches are noted as $K_C \leq K$ and no branch occurs when $K_C > K$. It is indicating that ahead K_C values, no branch exists. Reduced skin friction ($f''(0)$) raises when ϕ_{Cu} and K raises in stable branch, although it decreases in second branch when the-two applied parameters raise. A decreasing heat transfer ($-\theta'(0)$) decrease in the-two branches when ϕ_{Cu} enhances, though opposite movement is noticed while K enhances in the upper branch by keeping the constant values ϕ_{Cu}. It is observed that the porosity values are substantial to evaluate the existence of non-unique solutions. The various sort of velocity slip condition on $f''(0)$ is highlighted in Fig. 6. Partial kinds of slip conditions are examined in this study where δ shows the effect of the velocity slip condition of the first order and δ_T indicates the thermal slip effect of the first order. It is evidently pragmatic that no-slip condition (when $\delta = 0$) has a lower effect on the boundary layer separation of the hybrid nanofluid as compared to the velocity slip. The flow of hybrid fluid is flowed till a critical point S_{ci}, while no flow of fluid is possible when

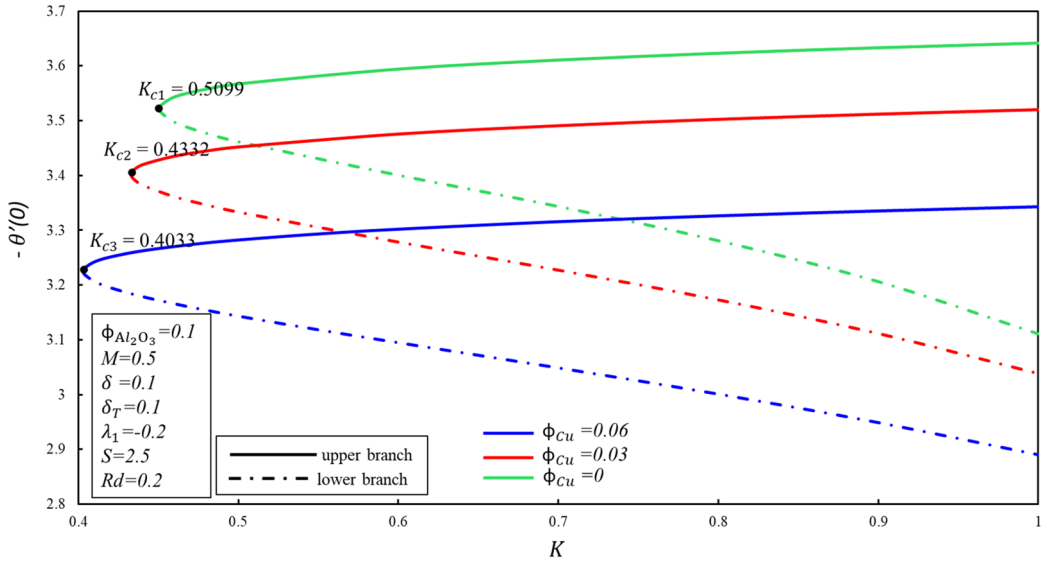

Figure 5. Behavior of $-\theta'(0)$ in impact of ϕ_{Cu}.

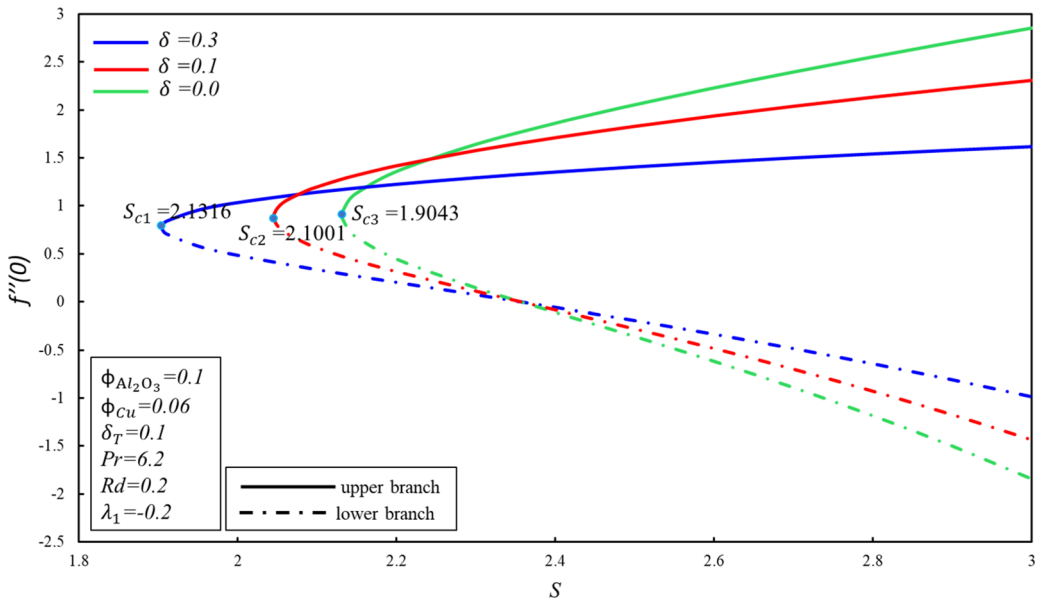

Figure 6. Behavior of $f''(0)$ in impact of δ.

$S < S_{ci}$. When suction velocity slip increase, skin friction increases (decreases) in upper branch. The lower branch of $f''(0)$ exhibits the inverse trend. Figure 7 demonstrates the effect of thermal (δ_T) slip with S on $-\theta'(0)$. Suction is often used to increase performance of diffusers with strong compression ratios of the flow. The thermal condition value is improved by developing the early layer separation. As it may be clearly seen, the magnitude of the thermal slip decreases because of suction before the critical value S_{ci} is raised. When $\delta_T = 0, 0.1, 0.3$, we have $S_{ci} = 2.0557, 2.0601, 2.0797$ respectively. It is noted that the branch duality occurs when $S < S_{ci}$ and no branch exists beyond S_{ci}. Heat transfer reduces in both branches when δ_T is improved. Substantially, this decreasing trend is due to the fact that heat is transferring fast from the surface to cold areas of the hybrid nanofluid.

Figures 8 and 9 display the variations of $f''(0)$ and $-\theta'(0)$ at different values of M. $M_c = 0.4513, 0.4353, 0.4073$ corresponds to the critical value of the parameter $\phi_{\mathrm{Cu}} = 0, 0.03, 0.06$, here M_c is the juncture where both branches meet. In the case of $M < M_c$, no branch occurs, and dual branches are marked as $M \geq M_C$. The boundary layer estimation is no longer reliable when the critical value is exceeded. Reduced skin friction $(f''(0))$ enhances when $\emptyset_2$ is enhanced in upper branch, whereas it reduces in lower branch. In addition, $f''(0)$ enhances in upper branch while M enhances by keeping fixed value of ϕ_{Cu}, although reverse movement is observed in lower branch. This fact is associated to cause that Lorenz force repressed the vortex developed by shrunk surface within boundary

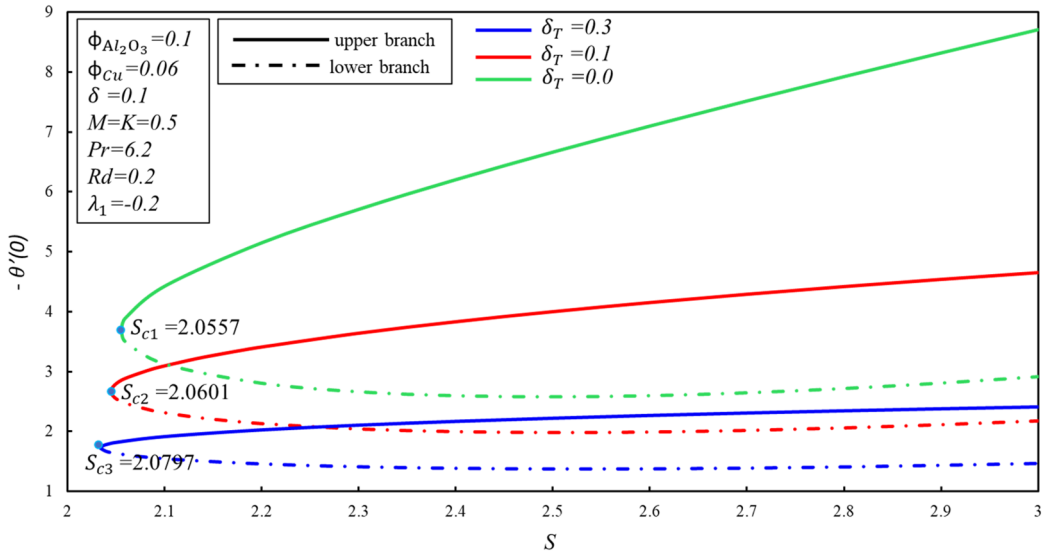

Figure 7. Behavior of $-\theta'(0)$ in impact of δ_T.

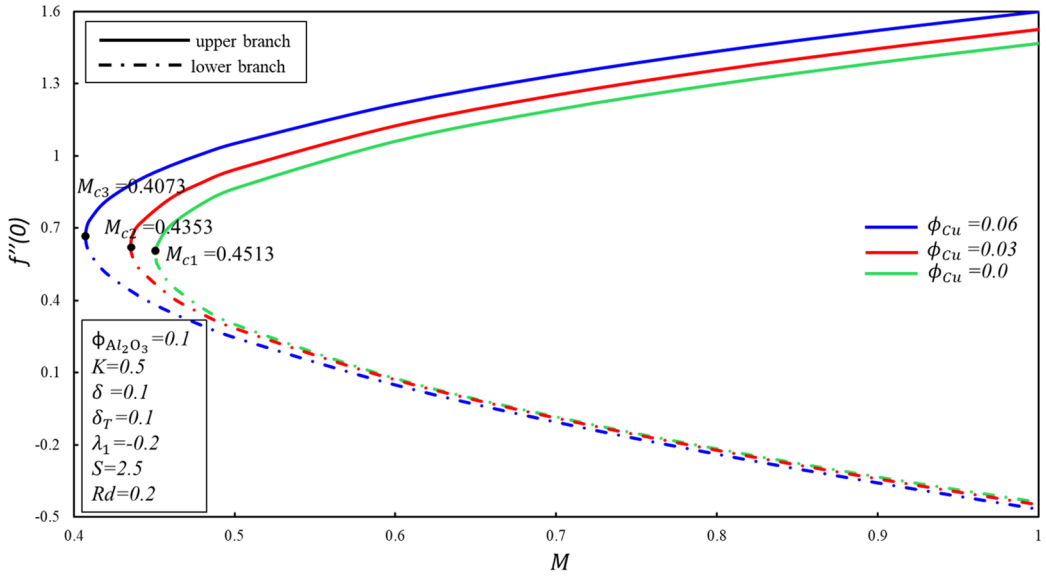

Figure 8. Behavior of $f''(0)$ in impact of ϕ_{Cu}.

layer. Reduced heat transfer $(-\theta'(0))$ enhances for upper branch when magnitude of M raises, although reverse movement is identified for lower branch. It should be noted that when $\phi_{\mathrm{Cu}} = 0$, the equations accept the alumina nanofluid model.

Figures 10 and 11 depict the effect of Rd on the velocity distribution $f'(\eta)$ and temperature distribution $\theta(\eta)$. These figures indicate that the boundary conditions for upper and lower branches are asymptotic and thus endorse the graphic findings stated in Figs. 2, 3, 4, 5, 6, 7, 8 and 9. It is worth mentioning here that triple branches exist in limited values of the applied parameters. See Fig. 10, three branches exist when $Rd = 0.5$. The velocity distribution for the lower branch decreases expressively while no change is observed in the upper branch. Additionally, it is noted that temperature distribution constantly rises in the upper and lower branches with a rising value of Rd. The plots of $f'(\eta)$ and $\theta(\eta)$ against λ_1 are shown in Figs. 12 and 13, respectively. It is revealed that the upper branch of $f'(\eta)$ and $\theta(\eta)$ neither increase nor decrease with the increasing values of λ_1, but $f'(\eta)$ and $\theta(\eta)$ are increasing functions of λ_1 for the lower branch. Besides, these graphs display that branches duality are conceivable for buoyancy assisting flow. On the other hand, a single branch exists for the opposing flow case. It is worth to define them here, assisting (opposing) flow happens when the force of buoyancy and the velocity of the surface are in the similar (opposite) direction. From Figs. 14 and 15, the decreasing behavior of upper branch of $f'(\eta)$ and $\theta(\eta)$ is observed. For $f'(\eta)$ $(\theta(\eta))$, lower branch increases (decreases) in the range of $2 \leq Pr \leq 4$ and

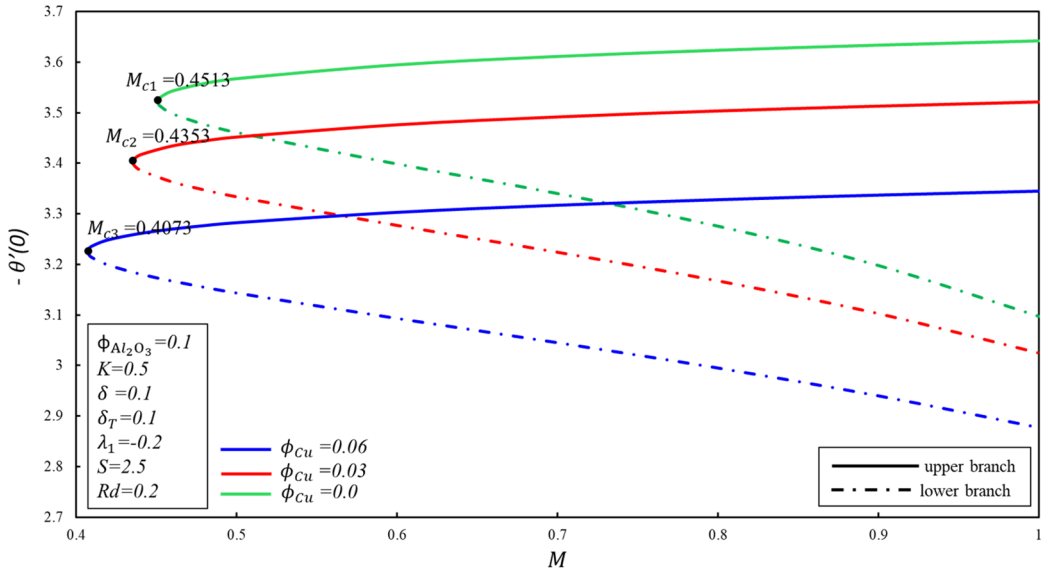

Figure 9. Behavior of $-\theta'(0)$ in impact of ϕ_{Cu}.

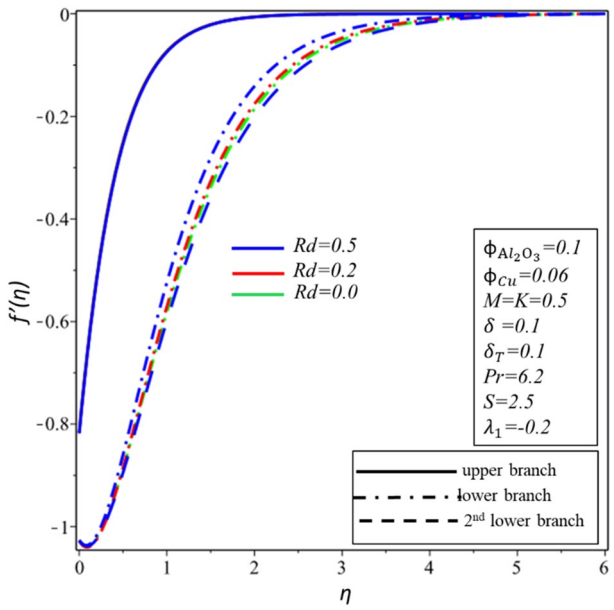

Figure 10. Behavior of $f'(\eta)$ in impact of Rd.

decreases (increases) in the range of $4 < Pr \leq 6.2$. Table 5 is constructed to display the values of the smallest eigenvalue ε_1. It is obtained from the table that upper branch is the stable one.

Conclusion

The radiative flow of hybrid nanofluid influences by multiple slip constraints has been addressed for vertical plate. The thermal results are observed with applications of mixed convection, magnetic force and porous media space. The thermal stability of model is checked and ensured. The validation of findings was carried out for limited situations where the current numerical outcomes have been well correlated with the previously published results.

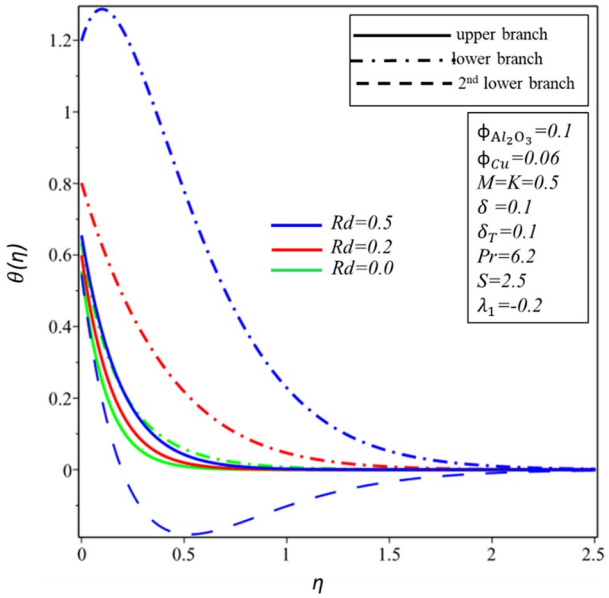

Figure 11. Behavior of $\theta(\eta)$ in impact of Rd.

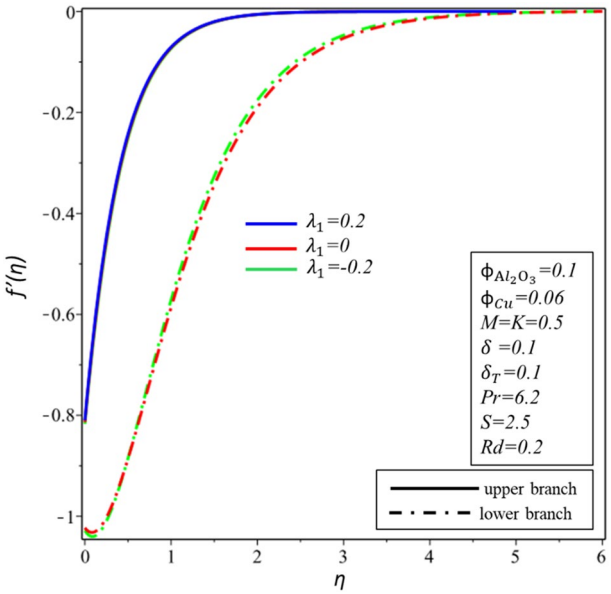

Figure 12. Behavior of $f'(\eta)$ in impact of λ_1.

- The hybrid nanoparticles addition comprehensively enhanced the characteristics of water base fluid.
- Dual even triple branches have been shown to be feasible with a confident range of applied parameters.
- The rate of heat transfer has decelerated with rising values of thermal slip condition. In addition, it has been revealed that the branches bifurcation has existed when $\lambda_1 = -0.2$.
- The flow of hybrid fluid is flowed till a critical point S_{ci}, while no flow of fluid is possible when $S < S_{ci}$.
- The study of temporal stability has revealed that only one of the two branches is reliable and stable, whilst the other is unreliable in the long term.

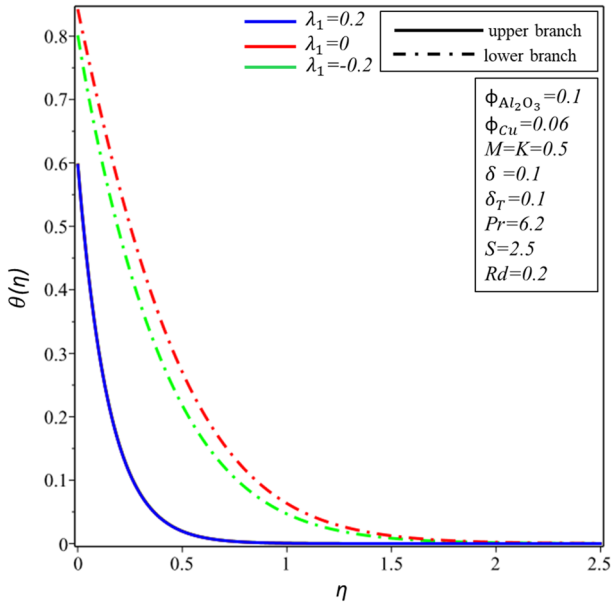

Figure 13. Behavior of $\theta(\eta)$ in impact of λ_1.

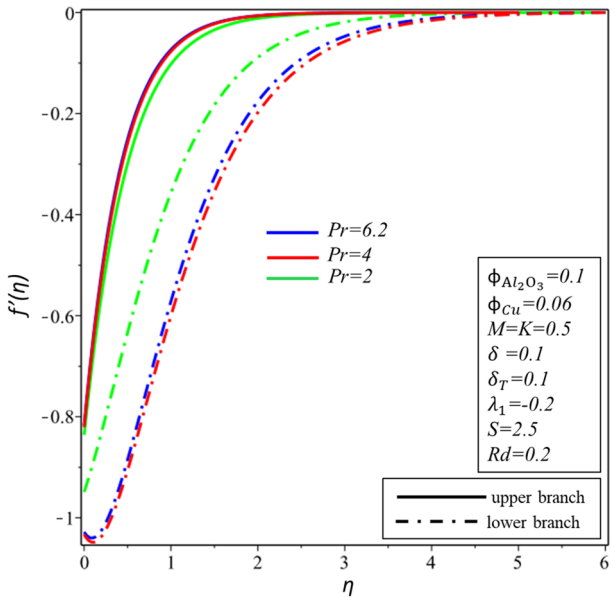

Figure 14. Behavior of $f'(\eta)$ in impact of Pr.

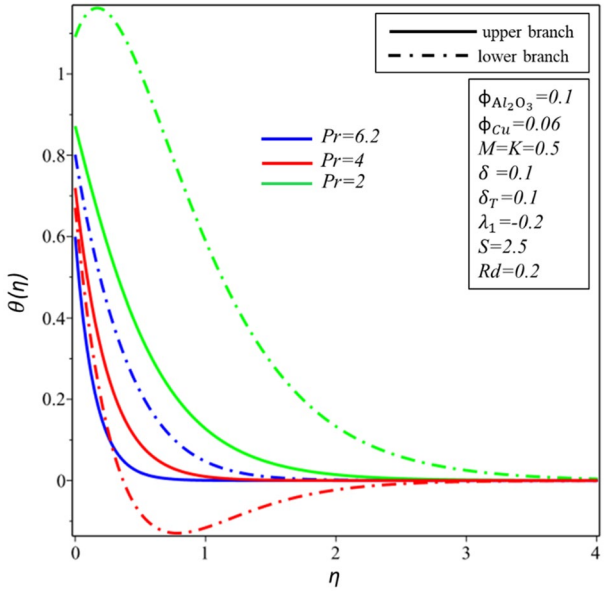

Figure 15. Behavior of $\theta(\eta)$ in impact of Pr.

	ε_1	
S	Upper branch	Lower branch
3	2.17111	− 1.9403
2.8	1.97369	− 1.7038
2.6	1.59794	− 1.4271
2.4	1.05140	− 0.9274
2.2	0.98623	− 0.86513
2.0447	0.00538	− 0.0948

Table 5. The numerical values of ε_1 for various values of suction where $\phi_{Al_2O_3} = 0.1, \phi_{Cu} = 0.06$, $\lambda_1 = -0.2, Rd = 0.2, \delta = \delta_T = 0.1$.

Data availability

The datasets used and/or analysed during the current study available from the corresponding author on reasonable request.

Received: 26 June 2022; Accepted: 21 September 2022
Published online: 30 September 2022

References

1. Hakeem, A. A., Renuka, P., Ganesh, N. V., Kalaivanan, R. & Ganga, B. Influence of inclined Lorentz forces on boundary layer flow of Casson fluid over an impermeable stretching sheet with heat transfer. *J. Magn. Magn. Mater.* **401**, 354–361 (2016).
2. Mandal, I. C. & Mukhopadhyay, S. Nonlinear convection in micropolar fluid flow past an exponentially stretching sheet in an exponentially moving stream with thermal radiation. *Mech. Adv. Mater. Struct.* **26**(24), 2040–2046 (2019).
3. Shahzad, A., Ali, R., Kamran, M. & Khan, S. U. D. Axisymmetric flow with heat transfer over exponentially stretching sheet: A computational approach. *Physica A* **554**, 124242 (2020).
4. Prasad, A. K. & Koseff, J. R. Combined forced and natural convection heat transfer in a deep lid-driven cavity flow. *Int. J. Heat Fluid Flow* **17**(5), 460–467 (1996).
5. Waini, I., Ishak, A. & Pop, I. Mixed convection flow over an exponentially stretching/shrinking vertical surface in a hybrid nanofluid. *Alex. Eng. J.* **59**(3), 1881–1891 (2020).
6. Al-Sumaily, G. F., Dhahadand, H. A. & Thompson, M. C. Mixed convection phenomenon in packed beds: A comprehensive review. *Therm. Sci. Eng. Prog.* **32**, 101242 (2022).
7. Merkin, J. H. Mixed convection boundary layer flow on a vertical surface in a saturated porous medium. *J. Eng. Math.* **14**(4), 301–313 (1980).
8. Merkin, J. H. On dual solutions occurring in mixed convection in a porous medium. *J. Eng. Math.* **20**(2), 171–179 (1986).
9. Ahmad, S. & Pop, I. Mixed convection boundary layer flow from a vertical flat plate embedded in a porous medium filled with nanofluids. *Int. Commun. Heat Mass Transf.* **37**(8), 987–991 (2010).
10. Choi, S. U. S. & Eastman, J. A. Enhancing thermal conductivity of fluids with nanoparticles. *ASME Fluids Eng. Div.* **231**, 99–105 (1995).

11. Avramenko, A. A. & Shevchuk, I. V. Lie group analysis and general forms of self-similar parabolic equations for fluid flow, heat and mass transfer of nanofluids. *J. Therm. Anal. Calorim.* **135**(1), 223–235 (2019).
12. Avramenko, A. A. & Shevchuk, I. V. *Modelling of Convective Heat and Mass Transfer in Nanofluids With and Without Boiling and Condensation* (Springer, 2022).
13. Punith Gowda, R. J. *et al.* Thermophoretic particle deposition in time-dependent flow of hybrid nanofluid over rotating and vertically upward/ downward moving disk. *Surf. Interfaces* **22**, 100864 (2021).
14. Naveen Kumar, R. *et al.* Impact of magnetic dipole on ferromagnetic hybrid nanofluid flow over a stretching cylinder. *Phys. Scr.* **96**, 045215 (2021).
15. Radhika, M., Punith Gowda, R. J., Naveenkumar, R. & Prasannakumara, B. C. Heat transfer in dusty fluid with suspended hybrid nanoparticles over a melting surface. *Heat Tranf.* **50**(3), 2150–2167 (2021).
16. Naveen Kumar, R., Punith Gowda, R. J., Gireesha, B. J. & Prasannakumara, B. C. Non-Newtonian hybrid nanofluid flow over vertically upward/downward moving rotating disk in a Darcy–Forchheimer porous medium. *Eur. Phys. J. Spec. Top.* **230**, 1227–1237 (2021).
17. Punith Gowda, R. J., Jyothi, A. M., Naveen Kumar, R., Prasannakumara, B. C., & Sarris, I. E. Convective flow of second grade fluid over a curved stretching sheet with Dufour and Soret effects. *Int. J. Appl. Comput. Math.* **7**, Article number: 226 (2021).
18. Gowda, R. J. P., Kumar, R. N., Jyothi, A. M., Prasannakumara, B. C. & Sarris, I. E. Impact of binary chemical reaction and activation energy on heat and mass transfer of marangoni driven boundary layer flow of a non-Newtonian nanofluid. *Processes* **9**(4), 702 (2021).
19. Haq, F. *et al.* Theoretical investigation of radiative viscous hybrid nanofluid towards a permeable surface of cylinder. *Chin. J. Phys.* **77**, 2761–2772 (2022).
20. Wang, Y. *et al.* Thermal outcomes for blood-based carbon nanotubes (SWCNT and MWCNTs) with Newtonian heating by using new Prabhakar fractional derivative simulations. *Case Stud. Therm. Eng.* **32**, 101904 (2022).
21. Lund, L. A., Omar, Z. & Khan, I. Quadruple solutions of mixed convection flow of magnetohydrodynamic nanofluid over exponentially vertical shrinking and stretching surfaces: Stability analysis. *Comput. Methods Programs Biomed.* **182**, 105044 (2019).
22. Yan, L. *et al.* Dual solutions and stability analysis of magnetized hybrid nanofluid with joule heating and multiple slip conditions. *Processes* **8**(3), 332 (2020).
23. Avramenko, A. A., Kobzar, S. G., Shevchuk, I. V., Kuznetsov, A. V. & Iwanisov, L. T. Symmetry of turbulent boundary layer flows: Investigation of different Eddy viscosity models. *Acta Mech.* **151**, 1–14 (2001).
24. Devi, S. A. & Devi, S. S. U. Numerical investigation of hydromagnetic hybrid Cu–Al_2O_3/water nanofluid flow over a permeable stretching sheet with suction. *Int. J. Nonlinear Sci. Numer. Simul.* **17**(5), 249–257 (2016).

Acknowledgements

The authors would like to thank the Deanship of Scientific Research at Umm Al-Qura University for supporting this work by Grant Code: 22UQU4331317DSR92. The authors express their gratitude to Princess Nourah bint Abdulrahman University Researchers Supporting Project (Grant No. PNURSP2022R152), Princess Nourah bint Abdulrahman University, Riyadh, Saudi Arabia. The authors acknowledge the financial support provided by the Center of Excellence in Theoretical and Computational Science (TaCS-CoE), KMUTT. This research was funded by National Science, Research and Innovation Fund (NSRF), and King Mongkut's University of Technology North Bangkok with Contract No. KMUTNB-FF-65-24.

Author contributions

Conceptualization, L. A. L. and U. Y.; methodology, L. A. L. and U. Y.; software, K. G.; validation, P. K. and M. I. K.; formal analysis, K. G.; investigation, S. U. K.; resources, P. Kumam; data curation, M. I. K.; writing—original draft preparation, S. U. K. and M. M. A.L.; writing—review and editing, K. G. and O. T B.; visualization, U. Y.; supervision, M. I. K.; project administration, M. I. K. and S. U. K.; funding acquisition, P. K. All authors have read and agreed to the published version of the manuscript.

Competing interests

The authors declare no competing interests.

Additional information

Correspondence and requests for materials should be addressed to M.I.K. or P.K.

Reprints and permissions information is available at www.nature.com/reprints.

Publisher's note Springer Nature remains neutral with regard to jurisdictional claims in published maps and institutional affiliations.